Title
Functional Analysis of the Bacteriophage T4 Rad50 Homolog (gp46) Coiled-coil Domain*

Journal
Journal of Biological Chemistry, 290(39)

ISSN
0021-9258

Authors
Barfoot, Tasida
Herdendorf, Timothy J
Behning, Bryanna R
et al.

Publication Date
2015-09-01

DOI
10.1074/jbc.m115.675132

Peer reviewed

THE JOURNAL OF BIOLOGICAL CHEMISTRY VOL. 290, NO. 39, pp. 23905–23915, September 25, 2015

Functional Analysis of the Bacteriophage T4 Rad50 Homolog (gp46) Coiled-coil Domain*

Received for publication, June 26, 2015, and in revised form, July 28, 2015 Published, JBC Papers in Press, August 4, 2015, DOI 10.1074/jbc.M115.675132

Tasida Barfoot[‡], Timothy J. Herdendorf[‡], Bryanna R. Behning[‡], Bradley A. Stohr[§1], Yang Gao[‡2], Kenneth N. Kreuzer[§], and Scott W. Nelson[‡3]

From the [‡]Department of Biochemistry, Biophysics, and Molecular Biology, Iowa State University, Ames, Iowa 50011 and the [§]Department of Biochemistry, Duke University Medical Center, Durham, North Carolina 27710

Background: The Mre11-Rad50 (MR) complex coordinates DNA double strand break repair.
Results: Mutations of the Rad50 coiled-coil disrupt the enzymatic functions of the MR complex.
Conclusion: The Rad50 coiled-coil regulates and mediates communication between the enzymatic domains of Rad50 and Mre11.
Significance: The Rad50 coiled-coil plays a more direct role in the enzymatic function of Rad50 and Mre11 than was previously assumed.

Rad50 and Mre11 form a complex involved in the detection and processing of DNA double strand breaks. Rad50 contains an antiparallel coiled-coil with two absolutely conserved cysteine residues at its apex. These cysteine residues serve as a dimerization domain and bind a Zn^{2+} cation in a tetrathiolate coordination complex known as the zinc-hook. Mutation of the zinc-hook in bacteriophage T4 is lethal, indicating the ability to bind Zn^{2+} is critical for the functioning of the MR complex. *In vitro*, we found that complex formation between Rad50 and a peptide corresponding to the C-terminal domain of Mre11 enhances the ATPase activity of Rad50, supporting the hypothesis that the coiled-coil is a major conduit for communication between Mre11 and Rad50. We constructed mutations to perturb this domain in the bacteriophage T4 Rad50 homolog. Deletion of the Rad50 coiled-coil and zinc-hook eliminates Mre11 binding and ATPase activation but does not affect its basal activity. Mutation of the zinc-hook or disruption of the coiled-coil does not affect Mre11 or DNA binding, but their activation of Rad50 ATPase activity is abolished. Although these mutants excise a single nucleotide at a normal rate, they lack processivity and have reduced repetitive exonuclease rates. Restricting the mobility of the coiled-coil eliminates ATPase activation and repetitive exonuclease activity, but the ability to support single nucleotide excision is retained. These results suggest that the coiled-coiled domain adopts at least two conformations throughout the ATPase/nuclease cycle, with one conformation supporting enhanced ATPase activity and processivity and the other supporting nucleotide excision.

Failure to properly detect and repair DNA double strand breaks (DSB)[4] in the genome can lead to chromosomal rearrangement, genome degradation, oncogenesis, and cell death (1). The necessity of a robust response to DSBs is underscored by the conservation of the Mre11-Rad50 (MR) complex across all domains of life (2). The MR complex localizes to DSBs shortly after their formation (3) and serves a number of enzymatic and architectural functions. The MR complex initiates the 5′ to 3′ resection that is required for homologous recombination (4) and microhomology-mediated end joining (5). Deletion of Mre11 or Rad50 causes embryonic lethality in mammals (4), and mutations in Mre11 are implicated in genetic disorders characterized by neural degeneration, oncogenesis, and hypersensitivity to radiation (6, 7). In bacteriophage T4, the MR complex is required for obligate recombination-dependent DNA replication after a short period of origin-mediated replication of the genome (8).

Mre11 is a Mn^{2+}-dependent nuclease that is composed of three structural domains (9). The capping and the nuclease domains are considered to make up the core structure of Mre11 (10). X-ray crystal structures of the MR complex reveal that the capping and nuclease domains interact with the N- and C-terminal lobes of Rad50, respectively (11–13). The C-terminal domain (CTD) of Mre11 is the smallest of the three domains but contains the largest Rad50-binding interface (12). Connecting the CTD to the capping domain is a flexible linker, which in the T4 system acts as an autoinhibitory element in the absence of Rad50 (14). *In vitro*, Mre11 is capable of single-stranded DNA endonuclease and dsDNA exonuclease activity in the 3′ to 5′ direction (11–13). The processive exonuclease activity of Mre11 requires the ATPase activity of Rad50 (15).

Rad50 is a member of the Structural Maintenance of Chromosomes family, which is a group of soluble ATP-binding cassette (ABC) enzymes that associate DNA in all domains of life

* This work was supported, in whole or in part, by National Institutes of Health Grant RO1 GM066934 (to K. N. K). This work was also supported by Carver Trust Young Investigator Grant 10-3603 (to S. W. N.), Iowa State University institutional support (to S. W. N), and National Science Foundation Grant MCB-1121693 (to S. W. N). The authors declare that they have no conflicts of interest with the contents of this article.

[1] Present address: Dept. of Pathology, University of California at San Francisco, San Francisco, CA 94143-0502.
[2] Present address: Laboratory of Molecular Biology, NIDDK, National Institutes of Health, 5 Memorial Dr., Rm. B1-03, Bethesda, MD 20892.
[3] To whom correspondence should be addressed. Tel.: 515-294-3434; Fax: 515-294-0453; E-mail: swn@iastate.edu.

[4] The abbreviations used are: DSB, double strand break; T4 phage, bacteriophage T4; 2AP, 2-aminopurine deoxyribonucleotide; SEC-MALS; size exclusion chromatography-multiangle light scattering; MR, Mre11/Rad50; IR, ionizing radiation; NBD, nucleotide binding domain; HEX, hexachlorofluorescein; ABC, ATP-binding cassette; CTD, C-terminal domain.

(16). Structural Maintenance of Chromosomes proteins have a common structure consisting of two halves of an ABC domain that are separated in sequence by an antiparallel coiled-coil (17, 18). The two halves of the ABC domain dimerize to form the nucleotide binding domain (NBD) that contains two ATP-active sites that are shared across the dimeric interface (19). The length of the coiled-coil in Rad50 varies from 250 amino acids in T4 phage to 900 amino acids in humans (2). A hinge domain is located at the apex of the coiled-coil, distal from the ABC domain, which serves as a second site of dimerization (20, 21). In Rad50, dimerization in this hinge domain occurs by tetrahedral coordination of a Zn^{2+} cation by absolutely conserved cysteine residues in the zinc-hook motif (C*XX*C) (20).

The precise role(s) of the Rad50 coiled-coil in MR complex function is unclear. In yeast, the phenotype of a zinc-hook deletion mutant is identical to that of complete Rad50 deficiency (22). Similarly, deletion or shortening of the coiled-coil eliminates both Spo11-induced DSB formation and telomere maintenance and greatly reduces the efficiency of homologous recombination (22). Most models for coiled-coil function involve its ability to physically link DNA strands to each other (20, 23–25). In eukaryotes, it has been proposed that the coiled-coil/zinc-hook domain of the MR complex tethers the ends of a DSB to the homologous sister chromatid that will be used as a template for homologous recombination-dependent DNA repair (26). Some models have multiple MR complexes bridging the two ends of the DSB to each other, as well as tethering the broken strands to the undamaged template (24). Genetic studies using the T4 phage system are consistent with this tethering arrangement. In T4, the two ends of the DSB are repaired in a coordinated manner so that a single homologous template is used to repair both ends of the DNA, even in the presence of a large number of available templates (27, 28). It is presumed that this end coordination is achieved through the physical tethering of the DSB ends to each other, likely through the coiled-coils of the MR complex. Depletion of T4 Rad50 results in reduced end coordination so that each end of the DSB invades different homologous templates (28, 29).

In addition to the role of the coiled-coil in bridging DNA strands, structural studies have suggested that the interaction between the CTD of Mre11 and the base of the Rad50 coiled-coil is a major route of communication between Rad50 and Mre11 (11, 12). The Rad50 coiled-coil is connected to the ATP active site through what has been termed the "signature coupling helices." ATP binding at the dimer interface of Rad50 causes the N-terminal domain to rotate, which causes the p-helix wedge to move between the signature coupling helices and spread them apart (11, 30). This movement is linked to the repositioning of the coiled-coil, which in turns alters the position of the Mre11 CTD by nearly 30 Å (11). As the CTD is connected to the main body of Mre11, it is reasonable to propose that the large movement of the CTD is transmitted through the flexible linker and cap domain to the Mre11 active site (30, 31).

To further clarify the function of the T4 Rad50 coiled-coil, we have investigated the *in vivo* and *in vitro* effects of its disruption by various means. Our purified Rad50 contains one tightly bound Zn^{2+} cation per dimer, and its removal via mutation of the zinc-hook has drastic effects. *In vivo*, the loss of Zn^{2+} binding is lethal and *in vitro* it broadly affects the enzymatic properties of the MR complex. Similarly, disruption of the coiled-coil via proline insertion or the introduction of a disulfide cross-link affects both ATPase and nuclease activity. Combining our results with an analysis of the Rad50 x-ray crystal structures in the apo and ATP-bound forms suggests the position of the coiled-coils may differentially regulate the ATPase and nuclease activities of Rad50 and Mre11, respectively.

Experimental Procedures

Analysis of CXXC Mutants in Vivo—We tested whether mutations in the C*XX*C motif of T4 Rad50 cause lethality as follows. Derivatives of plasmid pBR322 were constructed containing an EcoRI fragment of the T4 *46* gene (Rad50) using an overlap PCR strategy with appropriate primers. The PCR fragments were cleaved with EcoRI and ligated to EcoRI-linearized, phosphatase-treated pBR322 vector, generating the following protein/DNA sequences at the zinc-hook motif: 1) wild-type CPTC (TGT CCA ACC TGT); 2) SPTC (TCA CCA ACC TGT); 3) CPTS (TGT CCA ACC AGT); and 4) SPTS (TCA CCA ACC AGT). The identities of the plasmids were verified by DNA sequencing. Next, DH5α carrying each of the four plasmids was infected with T4 tdSG2-*46*^{am2}, a phage derivative carrying dual amber mutations in gene *46* at a multiplicity of infection of 3 (29). After a 90-min incubation at 37 °C, the phage lysates were harvested. Marker rescue from the plasmid can replace the dual-amber mutation region of gene *46* with the corresponding region of the plasmid, which contains the coding sequence of the CPTC region. The titer of gene *46am*$^{+}$ recombinants was determined by plating appropriate dilutions of each lysate on nonsuppressing *Escherichia coli* strain AB1 and the total titer by plating on *supD*-containing strain CR63.

Plasmid Construction and Mutagenesis—The $Rad50_{\Delta coil}$ construct was generated using a standard overlap PCR method to delete the coiled-coil and insert the codons for the "GGSEGGGSGEGGGTGS" linker between the N- and C-terminal domains of Rad50. The final PCR product was then subcloned into the pET28b expression vector. The C-terminal domain of T4 Mre11 (residues 290–339, $Mre11_{CTD}$, where $Mre11_{CTD}$ is a 49-amino acid peptide containing residues 290-339 of Mre11) was amplified using PCR and subcloned into the pTYB1 vector (15). The mutants $Rad50_{2CS}$ (C288S/C291S), $Rad50_{2KP}$ (K210P/K351P), and $Rad50_{xlink}$ (C312S/S183C) were generated using the Stratagene QuikChange® mutagenesis strategy. $Rad50_{C312S}$ was also generated and subjected to complete biochemical characterization. All constructs were verified by DNA sequencing.

Expression and Purification of Mre11 and Rad50 Proteins—T4 Mre11 and Rad50 were expressed and purified as described previously (15, 33). Purified proteins were concentrated to 60–200 μM. The extinction coefficients for determining the concentration of T4 Mre11, $Mre11_{CTD}$, Rad50, and $Rad50_{\Delta coil}$ are 69,130, 3,840, 33,140, and 20,340 cm^{-1} M^{-1}, respectively. Aliquots were flash-frozen with liquid nitrogen and stored at −80 °C. SDS-PAGE analysis was carried out using standard protocols (34) with 8% polyacrylamide/bisacrylamide at a 37.5:1 ratio. The gels were scanned

using a Bio-Rad ChemiDoc™ XRS+ system and analyzed using the ImageJ software (35).

Atomic Absorption Spectroscopy—The molar ratio of Zn^{2+} to Rad50 was measured by atomic absorption spectroscopy. Rad50 samples were dialyzed against a buffer solution of 400 mM sodium chloride and 20 mM Tris-HCl (pH 8.0) and diluted to 5 and 10 μM or 6 and 12 μM. Assuming a molar ratio of one Zn^{2+} ion per Rad50 dimer, these concentrations were predicted to fall within the range of standard solutions of 0.1–1 μg/ml zinc (1.5–15.3 μM) used to calibrate the instrument. The zinc concentration of each sample was measured on a 55B AA atomic absorption spectrometer (Agilent Technologies) with a 213.9 nm lamp. Measurements were made in triplicate, and the molar ratio of Rad50 molecules to zinc atoms was calculated for each sample.

Size Exclusion Chromatography-Multiangle Light Scattering (SEC-MALS)—Protein samples subjected to SEC-MALS analysis were injected into a Superdex™ 200 10/300 GL column in tandem with a Dawn Helios II multiangle light scattering detector (Wyatt Technology, Santa Barbara, CA) at a flow rate of 0.5 ml/min. All buffers contained 20 mM Tris-HCl (pH 7.9) and 400 mM sodium chloride. Buffers containing 1 mM ATP also contained 5 mM $MgCl_2$. Samples containing $Rad50_{S183C/C312S}$ in its reduced state were run using the standard buffer with 10 mM dithiothreitol (DTT). Data were analyzed using ASTRA 6 software (Wyatt Technology).

ATP Hydrolysis (ATPase) Kinetics—Steady-state ATPase activity was measured at 30 °C using a coupled assay linking ADP production to NADH oxidation (36). Each 300-μl reaction contained 50 mM Tris-HCl (pH 7.6), 50 mM KCl, 5 mM $MgCl_2$, 0.1 mg/ml BSA, 0.17 mM NADH, 1 mM phosphoenolpyruvate, pyruvate kinase (1.8 units), and lactose dehydrogenase (3 units) (Sigma). When present, Mre11 was kept at a slight excess over Rad50 (1.2-fold), and the DNA concentration used was at least 4-fold over the enzyme complex concentration. Reactions were started with the addition of Rad50 or MR complex, and the rate of change in NADH fluorescence was monitored at an emission wavelength of 460 nm (excitation wavelength of 340 nm) on a Cary Eclipse spectrofluorometer (Varian). Estimates of kinetic constants (k_{cat}, K_m, and Hill coefficient) were determined by fitting reaction velocities at various ATP concentrations to the Hill equation using SigmaPlot 10.0/Enzyme Kinetics Module 1.3 (Systat Software, Inc.).

DNA K_d Determination—The equilibrium binding constant of Rad50 for DNA was determined by the fluorescence anisotropy of the 50-bp DNA substrate 5′-labeled with hexachlorofluorescein (DNA_{HEX}). The dsDNA concentration was held constant at 10 nM, and the concentration of added Rad50 protein was varied from 0 to 12 μM in 50 mM Tris-HCl (pH 7.6), 50 mM KCl, and 5 mM $MgCl_2$. Anisotropy was measured on a Biotek Synergy Two 96-well plate reader with an excitation wavelength of 535 nm and an emission wavelength of 560 nm. Data were fit to a bimolecular equilibrium model using Dynafit (37).

Nuclease Assays—The nuclease products of Mre11-Rad50 complex were analyzed by denaturing PAGE. Each reaction contained 50 mM Tris-HCl (pH 7.6), 50 mM KCl, 5 mM $MgCl_2$, 0.3 mM $MnCl_2$, 0.1 mg/ml BSA, and 1.3 μM DNA_{HEX} and was started with the addition of 400 nM MR complex. When included, the ATP concentration was 1 mM. At specified time points, aliquots of the reaction were quenched in an equal volume of 100 mM EDTA, 50% formamide solution. Two microliters of each quenched solution were analyzed using 16% urea-PAGE (19:1 acrylamide/bisacrylamide). The gels were imaged using a Typhoon PhosphorImager with an excitation wavelength of 532 nm and a 555-nm bandpass filter for emission detection.

Position-specific nuclease activity was monitored by the release of the fluorescent adenine analog, 2-aminopurine (2AP) (38). A 50-bp dsDNA was constructed from 50 base oligonucleotides labeled at the 1- or 17-position from the 3′ end with 2AP. The intrinsic fluorescence of this nucleotide is quenched by base stacking, which is then relieved upon cleavage of the nucleotide from the DNA. Each 300-μl reaction contained 50 mM Tris-HCl (pH 7.6), 50 mM KCl, 5 mM $MgCl_2$, 0.3 mM $MnCl_2$, 0.1 mg/ml BSA, 1.3 μM 2AP of labeled DNA, and 0 or 1 mM ATP and was initiated by the addition of MR complex. Emission was monitored at 375 nm with an excitation wavelength of 310 nm in a Cary Eclipse spectrofluorometer (Varian). When 2AP was located at the 17-position relative to the 3′ end, the activity was measured over the initial 5 min of the reaction.

Results

Analysis of CXXC Mutants in Vivo—We constructed a series of four plasmids containing a 1-kb segment of T4 DNA with the C*XX*C-encoding region near the middle. In addition to the WT control, which encodes CPTC, we constructed otherwise identical plasmids with SPTC, CPTS, and SPTS. We then used a plasmid marker rescue approach to determine whether the single or double substitutions created a viable phage. In this approach, a conditional lethal gene *46* amber double-mutant phage infected the plasmid-bearing strains, and viable recombinants were selected on a nonsuppressing host. The dual gene *46* amber mutations are very near the CPTC-encoding region. Therefore, when plasmid-phage recombination replaces the amber mutations with plasmid-borne sequence to generate non-amber phage, the plasmid-borne CPTC region is usually also incorporated into the phage genome. With the WT plasmid, viable phage were generated at a frequency of about 2×10^{-4}, but each of the three mutant plasmids generated many fewer recombinants. The low frequency of viable phage from the mutant plasmids ($\sim 10^{-5}$) can be explained by multiple crossovers generating 46^+ phage. We sequenced four plaques arising from each of the three mutant plasmids, and all 12 were WT for the amber mutations and for the DNA encoding CPTC. We conclude that the fairly conservative cysteine to serine substitution at either location of the C*XX*C motif of T4 Rad50 results in a lethal mutation, *i.e.* completely or severely compromises the function of the T4 MR protein complex.

Rationale for Mutants Generated for Biochemical Characterization—The relative positions of the mutants that were generated and purified for this study are shown in Fig. 1, *A* and *B*. The $Rad50_{2CS}$ mutation was created to eliminate Zn^{2+} binding by the zinc-hook and corresponds to the SPTS construct used in the phage infections described above. The two cysteine residues that are mutated to serine in the $Rad50_{2CS}$ protein are

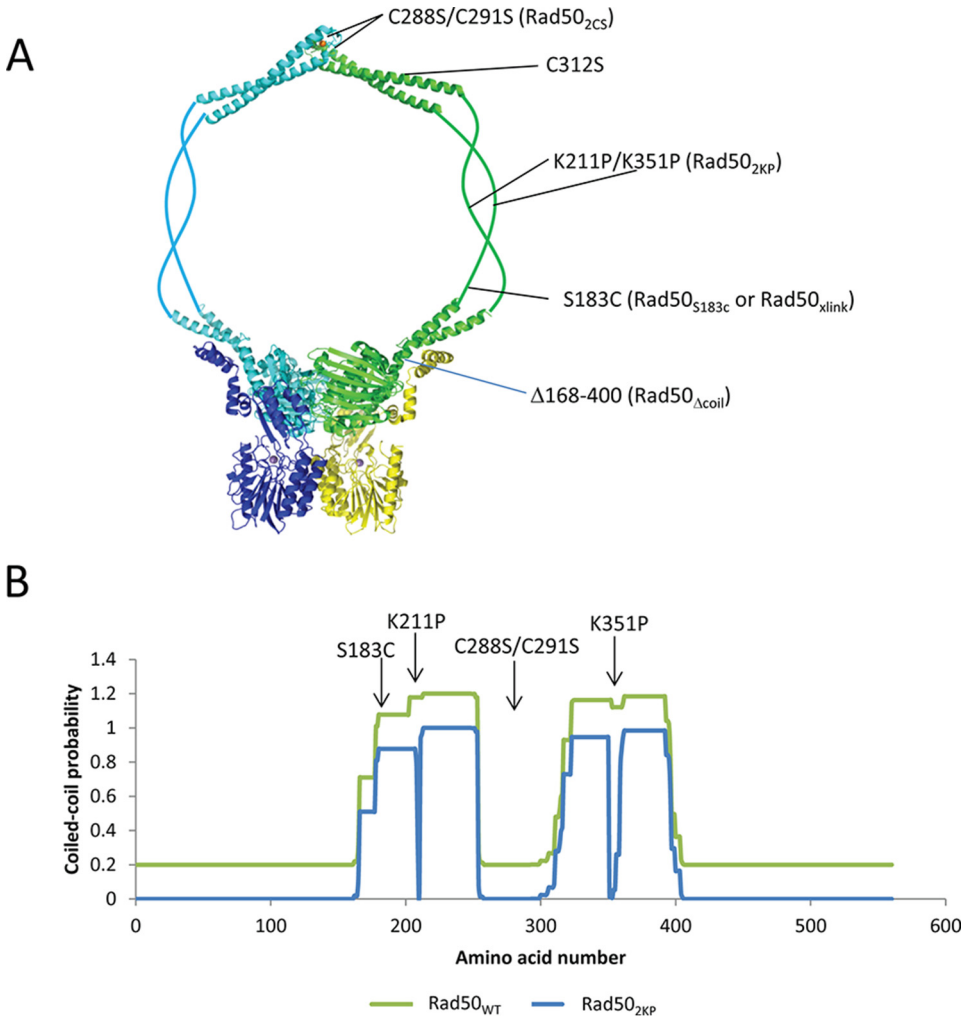

FIGURE 1. **Locations of characterized mutations of T4 Rad50.** *A,* Rad50 subunits are shown in *blue* and *cyan*, and the Mre11 subunits are shown in *blue* and *yellow*. The figure was generated using the x-ray crystal structures of the *P. furiosus* zinc-hook (20) and the *Thermotoga maritima* MR complex (12) (Protein Data Bank codes 1L8D and 3THO, respectively). The remainder of the coiled-coil is represented by the *thin lines* separating the head domain from the zinc-hook. The length of this section is proportional to the number of amino acids predicted to be in the coiled-coil of T4 Rad50. *B,* plot of coiled-coil probability *versus* the amino acid sequence of T4 Rad50$_{WT}$ (*green*) and Rad50$_{2KP}$ (*blue*). The probabilities were determined using the COILS server with a window width of 28 amino acids (41).

absolutely conserved in all Rad50 proteins and were previously known to affect the *in vivo* properties of the MR complex in other systems (22, 39, 40).

Rad50$_{2KP}$ was generated to disrupt the structure of the coiled-coil at a position that is approximately midway between the NBD and the zinc-hook. Fig. 1*B* shows a coiled-coil probability calculation for Rad50$_{WT}$ and Rad50$_{2KP}$ (41). This analysis predicts that the replacement of nonconserved lysine residues on the ascending and descending arms of the coiled-coil with proline will completely interrupt the structure.

The Rad50$_{S183C}$ protein was originally generated to measure the distance and/or movement of the coiled-coil using bifunctional cysteine-reactive cross-linkers. The serine at position 183 is poorly conserved and is positioned between the Rad50 NBD and the midway point of the ascending arm of the coiled-coil (Fig. 1). To specifically label Rad50$_{S183C}$, it would be necessary to mutate the single reactive cysteine that is present in T4 Rad50$_{WT}$, generating the Rad50$_{C312S}$ mutant. Assays using Ellman's reagent confirmed the loss of the reactive cysteine in Rad50$_{C312S}$, and a complete biochemical characterization indicated no significant differences relative to Rad50$_{WT}$ (data not shown). Although not explicitly stated hereafter, the Rad50$_{S183C}$ and Rad50$_{xlink}$ proteins contain the C312S mutation. Following the purification of Rad50$_{S183C}$, it was discovered that the mutant was unsuitable for cysteine labeling because a spontaneous disulfide bond forms during the purification process (see below).

Protein Purification—All proteins expressed to approximately the same degree and displayed similar affinity for the phosphocellulose column (binding at 200 mM NaCl and eluting at 400 mM). Each protein was purified a minimum of two times, and the biochemical properties of repeated protein preparations were not significantly different (*i.e.* less than ~25% change in all kinetic and binding constants). SDS-PAGE analysis indicated that the proteins were at least 90% pure; however, Rad50$_{S183C}$ appeared as two distinct bands when DTT was omitted from the loading buffer, indicating the formation of a disulfide bond (Fig. 2*A*). The mobility of the cross-linked protein in relation to the standards suggests that the molecular mass of the protein is near 200 kDa, which is most consistent

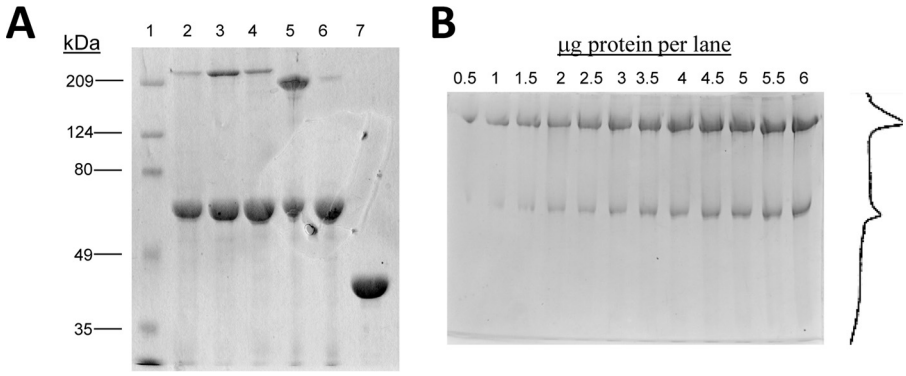

FIGURE 2. **Nonreducing SDS-polyacrylamide gel of purified mutant proteins.** *A,* 10 μg of protein were loaded in each lane. $Rad50_{S183C}$ was reduced using 1 mM DTT. *B,* increasing amounts of $Rad50_{xlink}$ analyzed using nonreducing SDS-PAGE. The amount of protein loaded in each lane is indicated *above* the gel. To the *right* of the gel is an example plot profile for the densitometric analysis of the *4 μg lane*. Analysis of all lanes gives an approximate cross-linked percentage of 79 ± 10%.

with a Rad50 trimer; however, both MALS (see below) and MALDI-TOF mass spectrometry (data not shown) indicate that the cross-linked species is dimeric. The cause of the aberrant mobility is unclear. Densitometric analysis of the protein indicates that ~78 ± 9% of the protein is in the cross-linked form (Fig. 2*B*). The nonreduced version of $Rad50_{S183C}$ will be referred to hereafter as $Rad50_{xlink}$ to indicate that it is predominantly in the cross-linked state. Although the analysis indicates that ~20% of the $Rad50_{xlink}$ is in the reduced state, the biochemical parameters for both ATPase and nuclease activity indicate that the observed activity is dominated by the cross-linked fraction (*e.g.* K_m-ATP for $Rad50_{xlink}$ is 10-fold elevated compared with $Rad50_{WT}$, see Table 4).

The WT and mutant proteins were then subjected to SEC-MALS analysis to determine their oligomeric state. $Rad50_{WT}$, $Rad50_{2CS}$, $Rad50_{xlink}$, and $Rad50_{S186C}$ eluted as a single peak (Fig. 3*A*), and the MALS analysis indicated that the proteins were in the dimeric form (Table 1). This indicates that the disulfide cross-link in $Rad50_{xlink}$ is intradimer, rather than between two or more Rad50 dimers, which would elute as a tetramer or higher oligomeric state. The elution profiles of $Rad50_{2KP}$ and $Rad50_{\Delta CC}$ are significantly different from the other Rad50 proteins (Fig. 3*A*). MALS analysis of the major peak for both of these proteins indicates that they are monomeric. Inclusion of ATP in the running buffer decreases their elution time and reproducibly increases their apparent molecular weight as determined by MALS (Table 1). This suggests that ATP binding promotes the dimerization of these mutants, but the monomer-dimer interconversion occurs in fast exchange relative to the time scale of the experiment (42). Because the apparent molecular weight is closer to that of the monomer, the equilibrium must lie in that direction.

Zn^{2+} Analysis—All Rad50 proteins were extensively dialyzed against three 2-liter changes of buffer prior to analysis using atomic absorption spectroscopy (Table 2). $Rad50_{WT}$ and $Rad50_{xlink}$ were found to contain approximately one Zn^{2+} cation per Rad50 dimer, whereas $Rad50_{2KP}$ and $Rad50_{2CS}$ contained negligible concentrations of Zn^{2+} when compared with a buffer control.

DNA and Mre11 Binding—The equilibrium dissociation constant of the Rad50 proteins for dsDNA (K_d-DNA) was measured using fluorescence anisotropy (Table 3). Similar to the

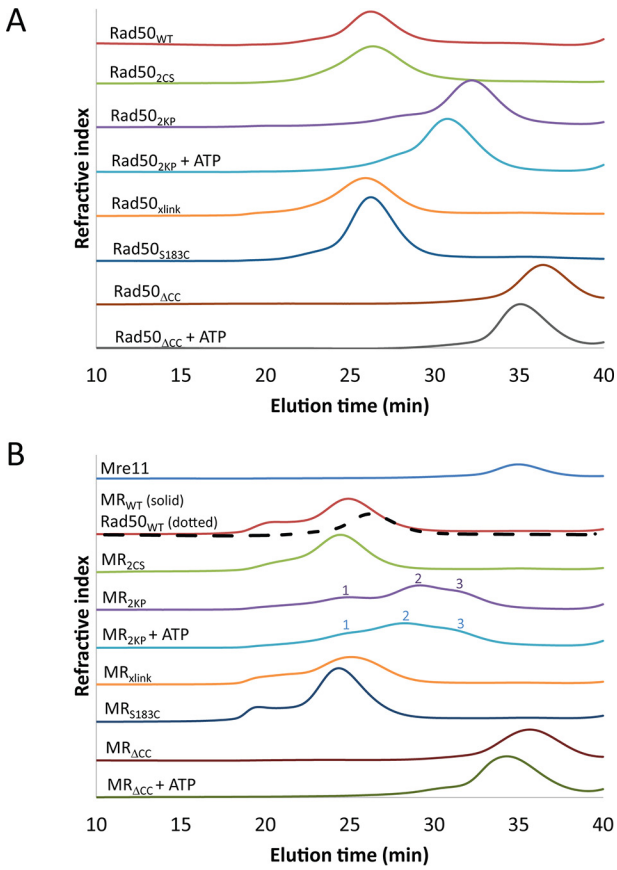

FIGURE 3. **SEC elution profiles of Rad50 proteins and MR complexes.** *A,* 100 μl of each Rad50 protein (50 μM) was applied to a Superdex™ 200 10/300 column at a flow rate of 0.5 ml/min. The elution profiles are scaled for ease of visualization. *B,* Rad50 + Mre11 (50 and 25 μM, respectively) were analyzed under the same conditions. The elution profile of Rad50 alone (*black dotted line*) has been added to the MR_{WT} profile (*red line*) to facilitate a direct comparison. As described under "Experimental Procedures," the molecular masses for the proteins and complexes in *A* and *B* were determined using MALS, and these values are reported in Table 1. With the exception of $Rad50_{2KP}$ and MR_{2KP}, the major peak of the elution profile was used in the analysis. In the case of $Rad50_{2KP}$ and MR_{2KP}, the molecular masses from the three peaks indicated were used. The *numbers* shown above the peak correspond to the numbers given in column 2 of Table 1.

Pyrococcus furiosus (Pfu) system, removal of the coiled-coil from T4 Rad50 results in a 100-fold increase in K_d-DNA, indicating a severe reduction in dsDNA binding affinity (43). Similarly, the $Rad50_{2KP}$ and $Rad50_{2CS}$ mutants also display reduced

TABLE 1

Molecular mass of Rad50 and MR complexes as determined by SEC-MALS

SEC-MALS experiments were performed in 20 mM Tris-HCl (pH 7.9), 400 mM NaCl.

Protein	Peak[a]	Mass	Standard error	Oligomeric state	Expected mass	Difference
		Da	*Da*		*Da*	*%*
$Rad50_{WT}$		146,300	1900	Homodimer	131,560	15.0
$Rad50_{2CS}$		133,000	2100	Homodimer	127,232	4.5
$Rad50_{2KP}$		57,760	860	Monomer	63,616	−9.2
$Rad50_{2KP}$ + ATP[b]		69,250	820	Monomer	63,616	8.9
$Rad50_{xlink}$		142,700	1400	Homodimer	127,232	16.6
$Rad50_{S183C}$[b]		133,400	1500	Homodimer	127,232	4.8
$Rad50_{\Delta CC}$		37,450	520	Monomer	38,332	−2.3
$Rad50_{\Delta CC}$ + ATP[b]		43,150	520	Monomer/dimer	38,332	12.6
Mre11		37,540	560	Monomer	39,168	−4.2
MR_{WT}		195,800	2500	Heterotetramer	205,568	−4.8
MR_{2CS}		196,300	2700	Heterotetramer	205,568	−4.5
MR_{2KP}	1	202,100	2400	Heterotetramer	205,568	−1.7
	2	84,960	1040	Heterodimer	102,784	−17.3
	3	70,130	990	Monomer (R)	65,616	6.9
MR_{2KP} + ATP[b]	1	194,900	2200	Heterotetramer	205,568	−5.2
	2	99,230	1100	Heterodimer	102,784	−3.5
	3	72,180	820	Monomer (R)	65,616	10.0
MR_{xlink}		189,700	2300	Heterotetramer	205,568	−7.7
$Rad50_{S183C}$[c]		133,400	1500	Homodimer	127,232	4.8
$MR_{\Delta CC}$		ND[d]		Monomer (R and M)		
$MR_{\Delta CC}$ + ATP[c]		ND		Monomer (R and M)		

[a] With the exception of MR_{2KP} and MR_{2KP} + ATP, the major peak of each elution profile shown in Fig. 3, *A* and *B,* was used for MALS analysis. For MR_{2KP} and MR_{2KP} + ATP, the indicated peak number corresponds to the numbering above the elution profiles shown on Fig. 3*B*.

[b] 1 mM ATP, 5 mM $MgCl_2$ was used.

[c] 10 mM dithiothreitol was used.

[d] ND means not determined. The peak contains a mixture of monomeric $Rad50_{\Delta CC}$ and Mre11.

TABLE 2

Molar ratio of Zn(II) to purified Rad50 protein

Protein	$[Zn^{2+}]/[Rad50]$[a]
MR_{WT}	0.45 ± 0.04
MR_{2CS}	0.04 ± 0.06
MR_{2KP}	0.06 ± 0.02
$Rad50_{xlink}$	0.45 ± 0.02

[a] The reported values are the average of at least three determinations and their associated standard deviations.

TABLE 3

WT and mutant Rad50 equilibrium binding constants for dsDNA

Polarization assays were performed in 50 mM Tris-HCl, 50 mM KCl, 0.1 mg/ml BSA (pH 7.6) in the presence of 5 mM $MgCl_2$ at room temperature. Protein concentrations ranged from 0 to 12 μM in each reaction with a DNA concentration of 10 nM. Values were determined by fitting data to simple equilibrium binding mechanisms using SigmaPlot software.

Protein	K_d-dsDNA
	nM
$Rad50_{WT}$	81 ± 8
$Rad50_{2CS}$	370 ± 40
$Rad50_{2KP}$	1600 ± 100
$Rad50_{\Delta coil}$	9300 ± 3600
$Rad50_{xlink}$	100 ± 25
$Rad50_{S183C}$	120 ± 30

affinity, with 20- and 4.5-fold increases in K_d-DNA, respectively. In contrast, the dsDNA affinity for $Rad50_{S183C}$ and $Rad50_{xlink}$ is nearly unchanged compared with $Rad50_{WT}$.

The ability of the Rad50 proteins to bind to Mre11 was assessed by SEC-MALS. An excess of Rad50 was incubated with Mre11 for several minutes at room temperature prior to separation via SEC and analysis by MALS (Fig. 3*B* and Table 1). Although T4 Mre11 alone is monomeric, two subunits bind to dimeric Rad50 to form a heterotetrameric complex (38, 44). With the exception of $Rad50_{\Delta coil}$, all Rad50 mutants bind Mre11, as measured by the disappearance of the Mre11 peak and the formation of a peak that elutes earlier than Rad50 alone. The MR complexes formed using $Rad50_{WT}$, $Rad50_{S183C}$, $Rad50_{xlink}$, and $Rad50_{2CS}$ elute at the expected time relative to the elution of standard proteins (data not shown), and MALS analysis indicates that the molecular masses of the eluted complexes are consistent with a heterotetramer (190–200 kDa, Table 1). Interestingly, with $Rad50_{2KP}$, the Mre11 peak is absent, indicating MR complex formation. However, three peaks are observed, and the MALS analysis indicates that both heterotetramers and heterodimers are formed along with monomeric $Rad50_{2KP}$. This indicates that Rad50 dimer formation is not a prerequisite to Mre11 binding. Similar to $Rad50_{2KP}$ alone, inclusion of ATP in the running buffer causes a slight decrease in the elution times of heterodimeric MR_{2KP} and monomeric $Rad50_{2KP}$, but it does not affect the heterotetrameric MR_{2KP}.

ATPase Kinetics—The kinetic constants for the ATPase reaction catalyzed by the isolated Rad50 mutants are relatively similar to $Rad50_{WT}$ (Table 4). This indicates that none of the mutants generated here significantly perturb the overall fold of the Rad50 NBD. In contrast to Rad50 in isolation, MR_{2CS}, MR_{2KP}, and MR_{xlink} show large differences compared with $Rad50_{WT}$ when Mre11 and DNA are present. Mre11-$Rad50_{\Delta coil}$ was not tested because the MALS analysis indicates that it does not interact with Mre11. $Rad50_{WT}$ shows a 30-fold increase in ATPase rate upon complex formation with Mre11 and DNA, whereas $Rad50_{2CS}$, $Rad50_{2KP}$, and $Rad50_{xlink}$ are unaffected by their presence (Table 4). The mutant complexes also display large decreases in cooperativity, with Hill coefficients of 1.2, 1.4, and 1.3 for MR_{2CS}, MR_{2KP}, and MR_{xlink}, respectively, compared with a Hill coefficient of 2.5 for MR_{WT}. Because the ATPase activity of MR_{xlink} is significantly reduced compared with MR_{WT}, we measured the effect of DTT addition to an ongoing reaction. As seen in Fig. 4*A*, the addition of DTT to the ongoing the reaction results in an immediate increase in the ATPase rate. To determine the kinetics of disulfide formation following reduction, MR_{xlink} was reduced with DTT

TABLE 4

Steady-state ATPase kinetic constants for WT and mutant Rad50 and MR complexes

Fluorometric assays were performed in 50 mM Tris-HCl, 50 mM KCl, 0.1 mg/ml BSA (pH 7.6) in the presence of 5 mM $MgCl_2$ at 30 °C. Values were determined by fitting data to a Hill equation. Errors represent the standard error of the fit. NA means not applicable.

Protein	k_{cat}-ATP	K_m-ATP	Hill coefficient	DNA activation[a]
	s^{-1}	μM		
$Rad50_{WT}$	0.088 ± 0.003	19 ± 1	1.3 ± 0.1	NA
$Rad50_{2CS}$	0.088 ± 0.005	22 ± 2	1.4 ± 0.2	NA
$Rad50_{2KP}$	.055 ± 0.003	190 ± 33	0.8 ± 0.1	NA
$Rad50_{\Delta coil}$	0.110 ± 0.008	133 ± 25	1.1 ± 0.2	NA
$Rad50_{xlink}$	0.038 ± 0.004	213 ± 49	1.4 ± 0.3	NA
$Rad50_{S183C}$	0.078 ± 0.003	233 ± 27	1.5 ± 0.2	NA
MR_{WT}-DNA	2.88 ± 0.05	57 ± 1	2.5 ± 0.1	33
MR_{2CS}-DNA	0.099 ± 0.004	38 ± 6	1.2 ± 0.2	1.1
MR_{2KP}-DNA	0.12 ± 0.007	193 ± 28	1.1 ± 0.1	2.2
$_{CTD}MR_{WT}$-DNA	0.55 ± 0.10	44 ± 2	1.6 ± 0.1	6.2
R_{WT}-DNA[b]	0.100 ± 0.003	54 ± 1	1.2 ± 0.1	1.1
MR_{xlink}-DNA	0.21 ± 0.04	439 ± 76	1.5 ± 0.2	5.5
MR_{S183C}-DNA	2.92 ± 0.12	118 ± 12	2.3 ± 0.4	5

[a] Fold increase in k_{cat} between the complex is indicated and Rad50 alone.
[b] Kinetic parameters were taken from Ref. 32.

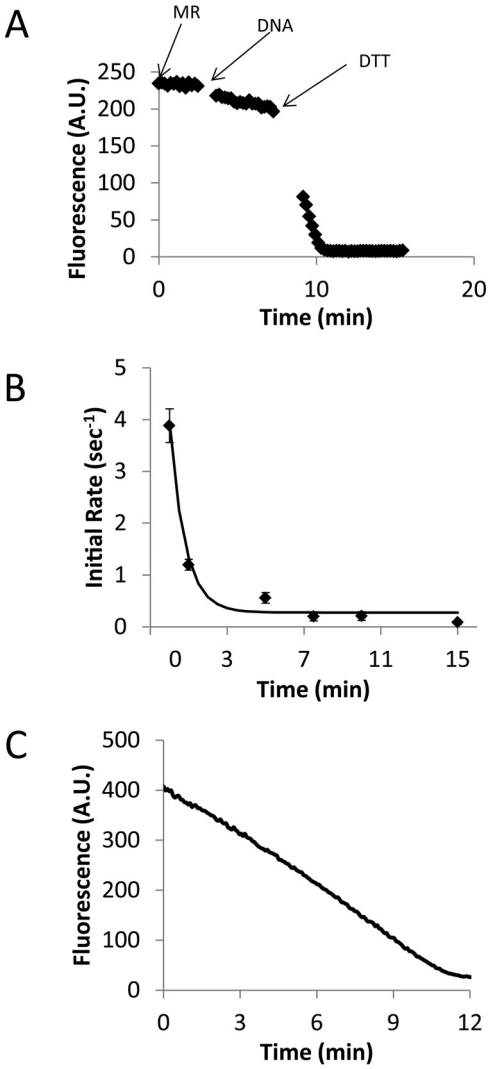

FIGURE 4. **Reduction and oxidation of $Rad50_{S183C}$.** *A,* ATPase time course. The additions of MR_{xlink}, DNA, and DTT are indicated. The *gaps* in the time course are due to the mixing time of the reaction after each addition. *B,* time course of $Rad50_{S183C}$ oxidation as described under "Experimental Procedures." The points are the average of three determinations with *error bars* indicating the standard deviation. The *solid line* is a single exponential fit of the data, which produces a rate constant of 1.3 min^{-1} with a standard error of 0.38 min^{-1}. *C,* time course of ATPase activity after 5 min of incubation under oxidizing conditions.

and then diluted into the ATPase assay buffer that lacked ATP but contained oxidized glutathione in excess of final DTT concentration. ATP was then added to the reaction at various time points, and the initial rate of ATPase activity served as a reporter of the oxidation state of $Rad50_{S183C}$. As seen in Fig. 4*B*, the rate of ATPase inactivation followed an exponential curve with a rate constant of 1.3 ± 0.38 min^{-1}. The progress curves were linear for up to 15 min following ATP addition, suggesting the presence of ATP inhibits further disulfide formation (Fig. 4*C*).

It is clear that alterations in the Rad50 coiled-coil directly affect the ATP active site of the NBD. Because the primary linkage between Mre11 and Rad50 is through the CTD of Mre11 and the base of the coiled-coil of Rad50, we examined the effect of the isolated Mre11 CTD ($Mre11_{CTD}$) on the ATP activity of Rad50. As seen in Fig. 5, the ATPase activity of Rad50 in complex with DNA and $Mre11_{CTD}$ resembles that of the complete MR_{WT} complex, with an 8-fold increase in k_{cat}-ATP and a Hill coefficient of 1.8 (Table 4). The addition of DNA to Rad50 does not result in activation of ATPase activity (15) indicating that the activation requires a minimal addition of DNA and the CTD of Mre11 (Table 4).

Nuclease Activity—To quantitatively determine the impact of the Rad50 mutations on the nuclease activity of the MR complex, we measured the rate of 2AP excision from the 1st and 17th positions relative to the 3′ end of the DNA (Table 5) (38). In the absence of ATP and with 2AP located at the 1st position, MR_{WT} and all mutants exhibit similar steady-state kinetics with apparent k_{cat} values ranging from 9.2 to 4.1 min^{-1}. When the probe is moved to the 17th position, ATP is now required for activity, and only MR_{S183C} behaves like MR_{WT} (apparent k_{cat} of 0.2 min^{-1}). The nuclease activities of MR_{2CS}, MR_{2KP}, and MR_{xlink} are 26-, 9-, and 13-fold reduced compared with MR_{WT} (Table 5).

To visually characterize the nuclease activity of Mre11 in complex with the Rad50 mutants, we analyzed the products of the nuclease assay using denaturing PAGE. Fluorescently labeled dsDNA was incubated with the MR complex, and samples of the reaction were quenched at time points spanning the course of 60 min (Fig. 6). In the absence of ATP, MR_{WT}, MR_{2CS}, and MR_{183C} have very similar activities, whereas MR_{2KP} and

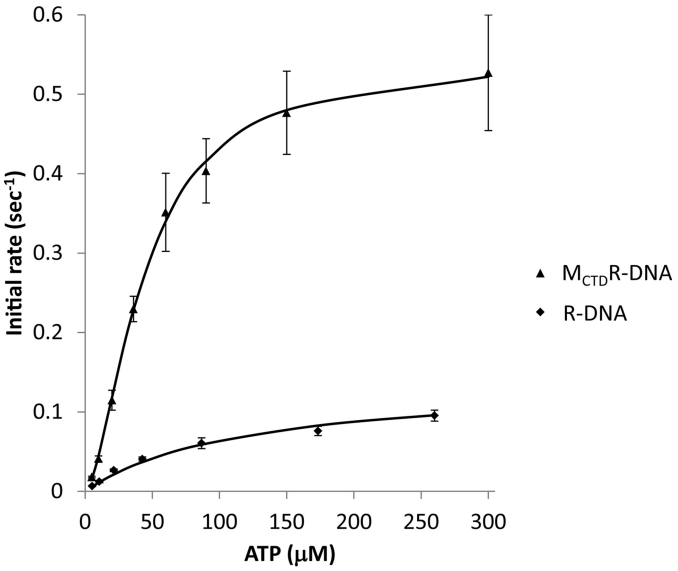

FIGURE 5. **Effect of ATP concentration on Rad50 ATPase activity.** The *black diamonds* and *triangles* represent data from the M_{CTD}R-DNA and the R-DNA complex, respectively. Each *data point* for M_{CTD}R-DNA and R-DNA represents the average of two or three determinations, respectively, and the *error bars* are the standard deviation. The *solid lines* are a fit of the data to the Hill equation with the resulting kinetic constants reported in Table 4.

TABLE 5

Steady-state nuclease activity of WT and mutant MR complexes

Fluorometric assays were performed in 50 mM Tris-HCl, 50 mM KCl, 0.1 mg/ml BSA (pH 7.6) in the presence of 5 mM $MgCl_2$ at 30 °C. Values were determined by fitting the slope of the reaction time course. The values represent the average of three determinations, and the errors represent the standard deviation. The concentration of ATP used was 1 mM.

Proteins	1-Position 2AP (−)ATP	17-Position 2AP (+)ATP
	min^{-1}	min^{-1}
MR_{WT}	2.25 ± 0.36	0.21 ± 0.04
MR_{2CS}	2.02 ± 0.08	0.008 ± 0.001
MR_{2KP}	0.61 ± 0.05	0.023 ± 0.004
$Rad50_{xlink}$	1.84 ± 0.21	0.0006 ± 0.0002
$Rad50_{S183C}$	1.06 ± 0.15	0.19 ± 0.035

MR_{xlink} are significantly reduced in their nuclease activity. A close inspection of the gel indicates that for both MR_{2KP} and MR_{xlink}, a single excision occurs relatively efficiently, but the rate of subsequent excisions is extremely reduced (especially so with MR_{xlink}).

The addition of ATP to the MR_{WT} complex reaction strongly activates its nuclease activity, with the appearance of short DNA products appearing at the earliest time points (Fig. 6). This is indicative of a highly processive reaction that includes a single rate-determining slow step prior to the onset of nuclease activity (expanded discussion can be found in Ref. 38). As expected, the ATP-dependent nuclease activity of MR_{S183C} is identical to MR_{WT}. In contrast, ATP reduces the nuclease activity of MR_{2CS}, MR_{2KP}, MR_{xlink} as compared with reactions in the absence of ATP. This behavior is often observed in mutant MR complexes with low ATPase activity or in the presence of nonhydrolyzable ATP (15, 44, 45). The inhibition may be due to the inability to dissociate from or translocate forward on the DNA substrate (*i.e.* the complex becomes stuck), or alternatively, slow ATP hydrolysis may prevent the binding of the complex to recessed ends.

Discussion

The function of the Rad50 coiled-coil has been the subject of intense research (22, 24, 25, 40, 43). Previous i*n vivo* experiments using the yeast model system indicate that the presence of the zinc-hook and a full-length coiled-coil are critical to the proper functioning of the MR complex (22, 40, 46). Here, we show that this is also true in the T4 system, as mutation of the zinc-hook cysteine residues is lethal, indicating that the ability to form a complex capable of DNA tethering is necessary for phage survival. In addition to these *in vivo* studies, electron microscopy (EM) and atomic force microscopy experiments have strongly supported a model where the coiled-coil and zinc-hook play an architectural role by physically tethering DNA strands to promote either homologous recombination or DNA end-joining (20, 23–25).

The effects of altering the zinc-hook and coiled-coil *in vivo* have most often been interpreted under the assumption that the enzymatic properties of the MR complex are unaffected, although recent work has suggested communication between the coiled-coil/zinc-hook and the globular domain (30, 40). The data presented here directly demonstrate this functional cross-talk. The coiled-coil is physically linked to the Rad50 active site through the signature coupling helices (11, 30). The mutants generated here, including the complete coiled-coil deletion, are largely unaffected in ATPase activity when measured in the absence of Mre11 and DNA, suggesting that there is minimal coupling between the coiled-coil and the ATP active site in the uncomplexed Rad50 dimer. In contrast, when Mre11 and dsDNA are bound, the disruption of the coiled-coil results in a loss of ATPase activation and a large decrease in cooperativity. These results suggest that the combined binding of Mre11 and DNA alter the position or reduce the flexibility of the coiled-coil, and these changes are transmitted allosterically to the ATP active site. As suggested by Petrini and co-workers (40), the coupling of the coiled-coil to the ATPase active site likely enables tethering-dependent regulation of ATP-dependent nuclease activity.

Eliminating Zn^{2+} binding by the zinc-hook through mutation ($Rad50_{2CS}$) appears to have no effect on the stability of the Rad50 dimer (Fig. 3*A*). This was somewhat unexpected, as other Rad50 homologs appear to have a relatively weak dimer interface in the absence of ATP (11, 12, 30). X-ray crystallography of an MR complex with the zinc-hook and most of the coiled-coil removed revealed an open form of the complex where the Rad50 subunits are separate and the Mre11 dimer interface maintains the heterotetrameric state of the complex (12). SAXS and disulfide cross-linking experiments using *P. furiosus* Rad50 suggest an equilibrium exists between open and closed forms of the MR complex in the absence of ATP (11, 30). This type of equilibrium may be unlikely in the T4 system because $Rad50_{2CS}$ is dimeric without ATP, indicating stable dimer formation does not require the zinc-hook. Additionally, unlike eukaryotic and archaeal Mre11, T4 Mre11 is monomeric in the absence of Rad50; therefore, it is difficult to envision the Mre11 dimer interface holding the MR complex in the open state (38).

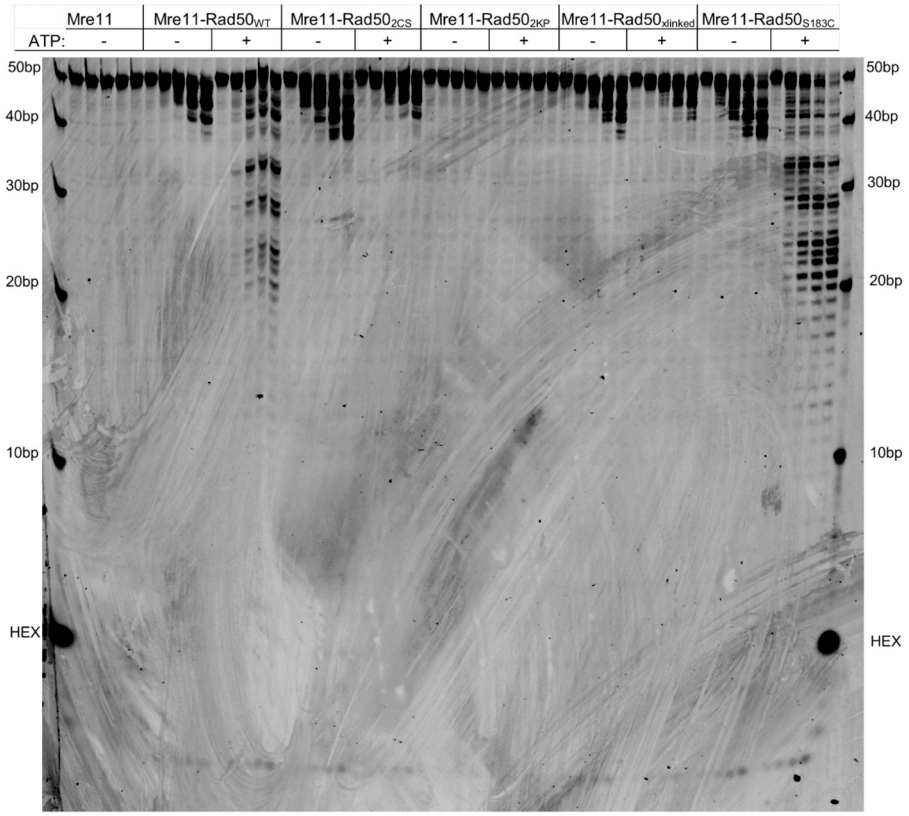

FIGURE 6. **Steady-state exonuclease activity visualized with urea-PAGE analysis.** The nuclease products of a 50-bp substrate labeled at the 5′ end with hexachlorofluorescein were visualized on a denaturing 16% polyacrylamide gel. Each assay contained 400 nM MR complex and 0 or 1 mM ATP. Samples were quenched at 0, 10, 20, 40, and 60 min.

The removal of the entire coiled-coil results in a monomeric protein (Fig. 3*A*), indicating that the coiled-coil itself and not solely the zinc-hook is an important factor for dimer stabilization. The presence or absence of the coiled-coil is likely communicated to the dimer interface via the signature coupling helices (11). This communication can also be seen in the $Rad50_{2KP}$ mutant. The coiled-coil perturbing proline residues appear to alter the conformation of Rad50 in the direction of the zinc-hook (because Zn^{2+} is poorly bound) and in the direction of the NBD (because ATPase activity is affected and dimerization is disrupted). The effect of the coiled-coil on Rad50 dimerization may explain the possible differences between the T4 MR complex and other homologs with regard to potential large scale changes in quaternary structure. T4 Rad50 has a relatively short coiled-coil (~250 amino acids) when compared with prokaryotes (~500), archaea (~600), and eukaryotes (~900). The longer coiled-coil in these other systems may allow Rad50 to adopt additional conformational states, including the open state seen in crystal structures and solution (12, 47, 48).

Perhaps the most unexpected result from this study was the spontaneous formation of a disulfide bond between the coiled-coils of the Rad50 dimer. This indicates that the coiled-coils come into close proximity, likely by adopting a parallel conformation. This parallel conformation can be seen in an unliganded Rad50 crystal structure (Protein Data Bank code 1II8 (45)) and in several EM and atomic force microscopy imaging studies (20, 24, 25, 32). These imaging experiments indicate that the coiled-coil is very dynamic, but it appears that the MR complex primarily adopts three conformations (20, 25). In the first conformation, the zinc-hooks from each Rad50 subunit come together in an intradimer fashion so that the coiled-coils form a ring-like structure. In the second conformation, the two coiled-coils are parallel and extended out from the NBD so that they are unresolvable and appear as a single rod. In the third conformation, the coiled-coils are again parallel, but the zinc-hooks participate in an inter-Rad50 dimer interaction so that the MR complex is hetero-octomeric. The latter two conformations would allow for the intra-dimer cross-linking of the coiled-coils that is seen in $Rad50_{xlink}$.

The reformation of the disulfide bond following reduction of $Rad50_{xlink}$ is relatively rapid, suggesting that the parallel conformation of the coiled-coils is a highly populated, or at a minimum the interconversion between the parallel and ring-like states occurs at a fast rate (regardless of where the equilibrium lies). We also observed that ATP binding and/or hydrolysis prevents further disulfide formation, as the ATPase time courses under oxidative conditions are linear over a course of several minutes. This suggests that bound ATP shifts the population of Rad50 conformers away from the parallel state, likely by stabilizing the ring-like state. The severely perturbed ATPase activity of $Rad50_{xlink}$ is consistent with this notion, as $Rad50_{xlink}$ has a low affinity for ATP and is a poor ATPase. The nuclease activity of $Rad50_{xlink}$ is consistent with defects in ATP binding and hydrolysis, as it is only able to perform nonprocessive nucleotide excisions. The 2AP-containing substrates confirm this, as

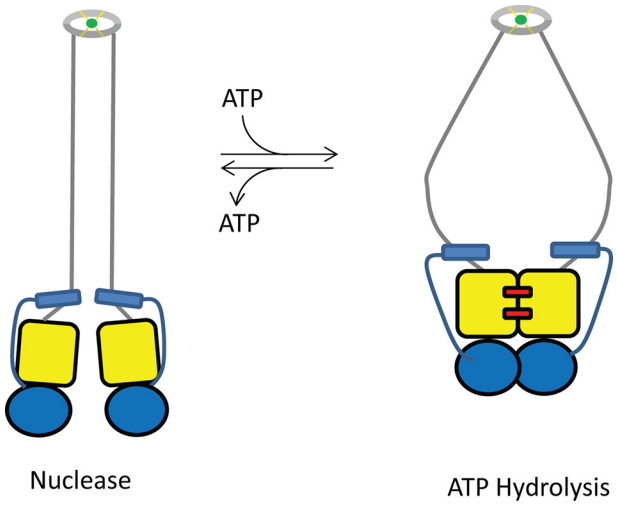

FIGURE 7. **Proposed two-state model for the MR complex.** Mre11, Rad50, and the Rad50 coiled-coil/zinc-hook domain are shown in *blue*, *yellow*, and *gray*, respectively. The bound Zn^{2+} cation and ATP are represented as a *green circle* and a *red rectangle*, respectively. The MR complex with parallel coils in close proximity (*left*) carries out the nucleotide excision reaction, whereas ATP binding promotes the ring-like coiled-coil conformation that carries out ATP hydrolysis (*right*). Additional details can be found under "Discussion."

the nuclease activity with the probe at the 1-position is nearly normal, whereas the 17-position is severely reduced.

Based on the enzymatic properties of the $Rad50_{xlink}$, we propose that the coiled-coils of the T4 MR complex alternate between parallel and ring-like states during its catalytic cycle. In this model, ATP binding and hydrolysis by Rad50 requires the ring-like state, whereas nucleotide excision by Mre11 occurs when the coiled-coils are in the parallel conformation (Fig. 7). Because Mre11 is connected to the coiled-coils via its CTD, the movement of the coiled-coils into the parallel conformation may drive the opening of the Mre11 dimer interface. This opening would then allow access to the otherwise protected nuclease active site (12, 31). This is consistent with our previous finding that disruption of the Mre11 dimer interface enhances the nuclease activity of the MR complex (38). The two states proposed here correspond well to two of the three conformational states proposed by Deshpande *et al.* (30) for the globular domain of the *P. furiosus* MR complex. In that model, ATP stabilizes a closed state that is capable of binding to dsDNA ends but has poor nuclease activity. ATP hydrolysis then promotes the formation of an intermediate state that is nuclease-competent. The third state proposed by Deshpande *et al.* (30) is an ATP-free open state that, as discussed above, may be unlikely in the T4 MR complex.

To alternate between the ring-like and parallel states, the zinc-hook region must also adopt different conformations. The structure of the zinc-hook from *P. furiosus* Rad50 shows the coiled-coils on either side of the Zn^{2+} at an angle of about 140° relative to each other (20). This orientation corresponds well to the ring-like state; however, it is difficult to envision this angle being retained in the parallel state. It is likely that the short unstructured regions between the end of the coiled-coil and the invariant cysteine residues of the zinc-hook act as a hinge that allows the coiled-coil to adopt either conformation.

The experiments described here have led us to suggest that the T4 MR complex may function somewhat differently from other MR complex homologs. Specifically, the properties of the T4 MR complex are not consistent with the open state that involves noninteracting Rad50 subunits. This difference may be the result of the shorter coiled-coil that presumably reduces the number of possible conformational states that the MR complex can adopt. It may, however, be due to differences in the preparation of purified proteins. We have found that purified T4 Rad50 contains a tightly bound Zn^{2+} cation that cannot be removed with extensive dialysis. EM imaging of human and *P. furiosus* MR complexes suggests that the affinity for Zn^{2+} is lower in these Rad50 homologs as compared with T4 and some of the conformational states that are observed may be due to the lack of Zn^{2+} bound to the zinc-hook (32). The biochemical and biophysical characterization of full-length MR complexes with bound and unbound Zn^{2+} from a wide variety of homologs will likely be necessary to determine whether there is a unified mechanism for all MR complexes.

Author Contributions—S. W. N. conceived and coordinated the study and assisted in the experiments in Fig. 4 and portions of Tables 4 and 5. T. B. performed and analyzed the experiments in Figs. 2, 3, and 6 and Tables 2 and 3, along with portions of Tables 1, 4, and 5. T. J. H. performed and analyzed the experiments in Tables 1, 4, and 5 and a portion of Fig. 5. B. R. B. performed and analyzed the experiments in Fig. 4 and portions of Tables 4 and 5. B. A. S. performed and analyzed the experiments related to the *in vivo* effects of the C*XX*C mutant. Y. G. performed and analyzed the experiment in a portion of Fig. 5. K. N. K. coordinated and conceived the experiments related to the *in vivo* effects of the C*XX*C mutant. All authors participated in the writing and editing of the paper. All authors reviewed the results and approved the final version of the manuscript.

References

1. Chapman, J. R., Taylor, M. R., and Boulton, S. J. (2012) Playing the end game: DNA double strand break repair pathway choice. *Mol. Cell* **47,** 497–510
2. Connelly, J. C., and Leach, D. R. (2002) Tethering on the brink: the evolutionarily conserved Mre11-Rad50 complex. *Trends Biochem. Sci.* **27,** 410–418
3. Petrini, J. H. (1999) The mammalian Mre11-Rad50-Nbs1 protein complex: integration of functions in the cellular DNA-damage response. *Am. J. Hum. Genet.* **64,** 1264–1269
4. Buis, J., Wu, Y., Deng, Y., Leddon, J., Westfield, G., Eckersdorff, M., Sekiguchi, J. M., Chang, S., and Ferguson, D. O. (2008) Mre11 nuclease activity has essential roles in DNA repair and genomic stability distinct from ATM activation. *Cell* **135,** 85–96
5. Decottignies, A. (2013) Alternative end-joining mechanisms: a historical perspective. *Front. Genet.* **4,** 48
6. Stewart, G. S., Maser, R. S., Stankovic, T., Bressan, D. A., Kaplan, M. I., Jaspers, N. G., Raams, A., Byrd, P. J., Petrini, J. H., and Taylor, A. M. (1999) The DNA double strand break repair gene hMRE11 is mutated in individuals with an ataxia-telangiectasia-like disorder. *Cell* **99,** 577–587
7. Carney, J. P., Maser, R. S., Olivares, H., Davis, E. M., Le Beau, M., Yates, J. R., 3rd, Hays, L., Morgan, W. F., and Petrini, J. H. (1998) The hMre11/hRad50 protein complex and Nijmegen breakage syndrome: linkage of double strand break repair to the cellular DNA damage response. *Cell* **93,** 477–486
8. Mosig, G., Gewin, J., Luder, A., Colowick, N., and Vo, D. (2001) Two recombination-dependent DNA replication pathways of bacteriophage T4, and their roles in mutagenesis and horizontal gene transfer. *Proc. Natl. Acad. Sci. U.S.A.* **98,** 8306–8311
9. Williams, R. S., Moncalian, G., Williams, J. S., Yamada, Y., Limbo, O., Shin,

D. S., Groocock, L. M., Cahill, D., Hitomi, C., Guenther, G., Moiani, D., Carney, J. P., Russell, P., and Tainer, J. A. (2008) Mre11 dimers coordinate DNA end bridging and nuclease processing in double-strand-break repair. *Cell* **135,** 97–109

10. Das, D., Moiani, D., Axelrod, H. L., Miller, M. D., McMullan, D., Jin, K. K., Abdubek, P., Astakhova, T., Burra, P., Carlton, D., Chiu, H.-J., Clayton, T., Deller, M. C., Duan, L., Ernst, D., *et al.* (2010) Crystal structure of the first eubacterial Mre11 nuclease reveals novel features that may discriminate substrates during DNA repair. *J. Mol. Biol.* **397,** 647–663
11. Williams, G. J., Williams, R. S., Williams, J. S., Moncalian, G., Arvai, A. S., Limbo, O., Guenther, G., SilDas, S., Hammel, M., Russell, P., and Tainer, J. A. (2011) ABC ATPase signature helices in Rad50 link nucleotide state to Mre11 interface for DNA repair. *Nat. Struct. Mol. Biol.* **18,** 423–431
12. Lammens, K., Bemeleit, D. J., Möckel, C., Clausing, E., Schele, A., Hartung, S., Schiller, C. B., Lucas, M., Angermüller, C., Söding, J., Strässer, K., and Hopfner, K.-P. (2011) The Mre11:Rad50 structure shows an ATP-dependent molecular clamp in DNA double strand break repair. *Cell* **145,** 54–66
13. Lim, H. S., Kim, J. S., Park, Y. B., Gwon, G. H., and Cho, Y. (2011) Crystal structure of the Mre11-Rad50-ATPγS complex: understanding the interplay between Mre11 and Rad50. *Genes Dev.* **25,** 1091–1104
14. Gao, Y., and Nelson, S. W. (2014) Autoinhibition of bacteriophage T4 Mre11 by its C-terminal domain. *J. Biol. Chem.* **289,** 26505–26513
15. Herdendorf, T. J., Albrecht, D. W., Benkovic, S. J., and Nelson, S. W. (2011) Biochemical characterization of bacteriophage T4 Mre11/Rad50 complex. *J. Biol. Chem.* **286,** 2382–2392
16. Jones, P. M., O'Mara, M. L., and George, A. M. (2009) ABC transporters: a riddle wrapped in a mystery inside an enigma. *Trends Biochem. Sci.* **34,** 520–531
17. Hopfner, K. P., and Tainer, J. A. (2003) Rad50/SMC proteins and ABC transporters: unifying concepts from high-resolution structures. *Curr. Opin. Struct. Biol.* **13,** 249–255
18. Alani, E., Subbiah, S., and Kleckner, N. (1989) The yeast RAD50 gene encodes a predicted 153-kD protein containing a purine nucleotide-binding domain and two large heptad-repeat regions. *Genetics* **122,** 47–57
19. Hopfner, K. P., Karcher, A., Shin, D. S., Craig, L., Arthur, L. M., Carney, J. P., and Tainer, J. A. (2000) Structural biology of Rad50 ATPase: ATP-driven conformational control in DNA double strand break repair and the ABC-ATPase superfamily. *Cell* **101,** 789–800
20. Hopfner, K.-P., Craig, L., Moncalian, G., Zinkel, R. A., Usui, T., Owen, B. A., Karcher, A., Henderson, B., Bodmer, J.-L., McMurray, C. T., Carney, J. P., Petrini, J. H., and Tainer, J. A. (2002) The Rad50 zinc-hook is a structure joining Mre11 complexes in DNA recombination and repair. *Nature.* **418,** 562–566
21. Harvey, S. H., Krien, M. J., and O'Connell, M. J. (2002) Structural maintenance of chromosomes (SMC) proteins, a family of conserved ATPases. *Genome Biol.* **3,** REVIEWS3003
22. Hohl, M., Kwon, Y., Galván, S. M., Xue, X., Tous, C., Aguilera, A., Sung, P., and Petrini, J. H. (2011) The Rad50 coiled-coil domain is indispensable for Mre11 complex functions. *Nat. Struct. Mol. Biol.* **18,** 1124–1131
23. Anderson, D. E., Trujillo, K. M., Sung, P., and Erickson, H. P. (2001) Structure of the Rad50 × Mre11 DNA repair complex from *Saccharomyces cerevisiae* by electron microscopy. *J. Biol. Chem.* **276,** 37027–37033
24. de Jager, M., van Noort, J., van Gent, D. C., Dekker, C., Kanaar, R., and Wyman, C. (2001) Human Rad50/Mre11 is a flexible complex that can tether DNA ends. *Mol. Cell* **8,** 1129–1135
25. Moreno-Herrero, F., de Jager, M., Dekker, N. H., Kanaar, R., Wyman, C., and Dekker, C. (2005) Mesoscale conformational changes in the DNA-repair complex Rad50/Mre11/Nbs1 upon binding DNA. *Nature* **437,** 440–443
26. Assenmacher, N., and Hopfner, K.-P. (2004) MRE11/RAD50/NBS1: complex activities. *Chromosoma* **113,** 157–166
27. Stohr, B. A., and Kreuzer, K. N. (2002) Coordination of DNA ends during double-strand-break repair in bacteriophage T4. *Genetics* **162,** 1019–1030
28. Shcherbakov, V. P., Plugina, L., Shcherbakova, T., Sizova, S., and Kudryashova, E. (2006) Double strand break repair in bacteriophage T4: coordination of DNA ends and effects of mutations in recombinational genes. *DNA Repair* **5,** 773–787
29. Almond, J. R., Stohr, B. A., Panigrahi, A. K., Albrecht, D. W., Nelson, S. W., and Kreuzer, K. N. (2013) Coordination and processing of DNA ends during double strand break repair: the role of the bacteriophage T4 Mre11/Rad50 (MR) complex. *Genetics* **195,** 739–755
30. Deshpande, R. A., Williams, G. J., Limbo, O., Williams, R. S., Kuhnlein, J., Lee, J.-H., Classen, S., Guenther, G., Russell, P., Tainer, J. A., and Paull, T. T. (2014) ATP-driven Rad50 conformations regulate DNA tethering, end resection, and ATM checkpoint signaling. *EMBO J.* **33,** 482–500
31. Möckel, C., Lammens, K., Schele, A., and Hopfner, K.-P. (2012) ATP driven structural changes of the bacterial Mre11:Rad50 catalytic head complex. *Nucleic Acids Res.* **40,** 914–927
32. de Jager, M., Trujillo, K. M., Sung, P., Hopfner, K. P., Carney, J. P., Tainer, J. A., Connelly, J. C., Leach, D. R., Kanaar, R., and Wyman, C. (2004) Differential arrangements of conserved building blocks among homologs of the Rad50/Mre11 DNA repair protein complex. *J. Mol. Biol.* **339,** 937–949
33. Herdendorf, T. J., and Nelson, S. W. (2014) Catalytic mechanism of bacteriophage T4 Rad50 ATP hydrolysis. *Biochemistry* **53,** 5647–5660
34. Laemmli, U. K. (1970) Cleavage of structural proteins during the assembly of the head of bacteriophage T4. *Nature* **227,** 680–685
35. Schneider, C. A., Rasband, W. S., and Eliceiri, K. W. (2012) NIH Image to ImageJ: 25 years of image analysis. *Nat. Methods* **9,** 671–675
36. Gilbert, S. P., and Mackey, A. T. (2000) Kinetics: a tool to study molecular motors. *Methods* **22,** 337–354
37. Kuzmic, P. (1996) Program DYNAFIT for the analysis of enzyme kinetic data: application to HIV proteinase. *Anal. Biochem.* **237,** 260–273
38. Albrecht, D. W., Herdendorf, T. J., and Nelson, S. W. (2012) Disruption of the bacteriophage T4 Mre11 dimer interface reveals a two-state mechanism for exonuclease activity. *J. Biol. Chem.* **287,** 31371–31381
39. He, J., Shi, L. Z., Truong, L. N., Lu, C.-S., Razavian, N., Li, Y., Negrete, A., Shiloach, J., Berns, M. W., and Wu, X. (2012) Rad50 zinc hook is important for the Mre11 complex to bind chromosomal DNA double-stranded breaks and initiate various DNA damage responses. *J. Biol. Chem.* **287,** 31747–31756
40. Hohl, M., Kochańczyk, T., Tous, C., Aguilera, A., Krężel, A., and Petrini, J. H. (2015) Interdependence of the rad50 hook and globular domain functions. *Mol. Cell.* **57,** 479–491
41. Lupas, A., Van Dyke, M., and Stock, J. (1991) Predicting coiled coils from protein sequences. *Science.* **252,** 1162–1164
42. Gell, D. A., Grant, R. P., and Mackay, J. P. (2012) The detection and quantitation of protein oligomerization. *Adv. Exp. Med. Biol.* **747,** 19–41
43. Lee, J.-H., Mand, M. R., Deshpande, R. A., Kinoshita, E., Yang, S.-H., Wyman, C., and Paull, T. T. (2013) Ataxia telangiectasia-mutated (ATM) kinase activity is regulated by ATP-driven conformational changes in the Mre11/Rad50/Nbs1 (MRN) complex. *J. Biol. Chem.* **288,** 12840–12851
44. Herdendorf, T. J., and Nelson, S. W. (2011) Functional evaluation of bacteriophage T4 Rad50 signature motif residues. *Biochemistry* **50,** 6030–6040
45. De la Rosa, M. B., and Nelson, S. W. (2011) An interaction between the Walker A and D-loop motifs is critical to ATP hydrolysis and cooperativity in bacteriophage T4 Rad50. *J. Biol. Chem.* **286,** 26258–26266
46. Wiltzius, J. J., Hohl, M., Fleming, J. C., and Petrini, J. H. (2005) The Rad50 hook domain is a critical determinant of Mre11 complex functions. *Nat. Struct. Mol. Biol.* **12,** 403–407
47. Lafrance-Vanasse, J., Williams, G. J., and Tainer, J. A. (2015) Envisioning the dynamics and flexibility of Mre11-Rad50-Nbs1 complex to decipher its roles in DNA replication and repair. *Prog. Biophys. Mol. Biol.* **117,** 182–193
48. Wyman, C., Lebbink, J., and Kanaar, R. (2011) Mre11-Rad50 complex crystals suggest molecular calisthenics. *DNA Repair* **10,** 1066–1070